

AD-A191 178

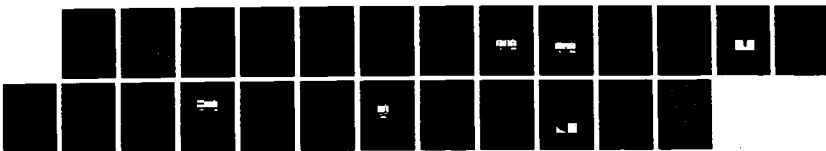
NONLINEAR WAVE PROPAGATION IN FREE ELECTRON LASERS(U)  
BERKELEY RESEARCH ASSOCIATES INC CA W B COLSON  
31 DEC 86 BRA-88-328R N00014-85-C-0493

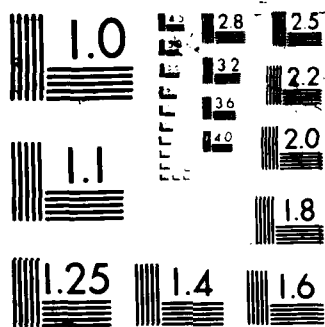
1/1

UNCLASSIFIED

F/G 9/3

NL





4

DTIC FILE



**BERKELEY RESEARCH  
ASSOCIATES, INC.**

**AD-A191 178**

BRA-88-328R

**NONLINEAR WAVE PROPAGATION IN  
FREE ELECTRON LASERS**

**W. B. Colson  
Berkeley Research Associates, Inc.  
P. O. Box 241  
Berkeley, CA 94701**

**Final Scientific Report  
Contract No. N00014-85-C-0493**

**Prepared for  
Office of Naval Research  
Physics Division  
800 N. Quincy Street  
Arlington, VA 22217  
Attn: Dr. H. Pilloff**

**DTIC  
ELECTE  
FEB 09 1988  
S a H D**

**DISTRIBUTION STATEMENT A**

**Approved for public release;  
Distribution unlimited.**

**88 2 01 08 6**

BRA-88-328R

**NONLINEAR WAVE PROPAGATION IN  
FREE ELECTRON LASERS**

**W. B. Colson  
Berkeley Research Associates, Inc.  
P. O. Box 241  
Berkeley, CA 94701**

**Final Scientific Report  
Contract No. N00014-85-C-0493**

**Prepared for  
Office of Naval Research  
Physics Division  
800 N. Quincy Street  
Arlington, VA 22217  
Attn: Dr. H. Pilloff**

RE: Distribution Statement  
Approved for Public Release. Distribution  
Unlimited.  
Per Dr. Herschel S. Pilloff,, ONR/Code 1112LO



Accession For	
NTIS GRA&I	<input checked="checked" type="checkbox"/>
DTIC TAB	<input type="checkbox"/>
Unannounced	<input type="checkbox"/>
Distribution	
a. <i>per Telecom</i>	
Distribution/	
Availability Codes	
Avail and/or	
Dist	Special
A-1	

Final Scientific Report  
Office of Naval Research N00014-85-C-0493  
July 1, 1985 to December 31, 1986  
W. B. Colson

**Scientific Progress Report:**

Below is an outline of the research progress during this contracting period and the effort to present that work in journal publications. New research results were found in the FEL klystron theory, exotic short-pulse evolution, optical guiding in the high-gain regime, fully four-dimensional simulations of the FEL, coherence development and line-narrowing in the FEL, and a global map describing the trapped-particle instability and chaos regions in the FEL. Two review papers describe the development and fundamentals of FEL theory and experiment. The theoretical foundations covered in the review papers were, in large part, supported by the Office of Naval Research over several years in this program.

**Self-Consistent FEL Klystron Theory**

In collaboration with I. Boscolo, the description of the high-gain klystron FEL was improved. Previous work has assumed low-gain in the analysis of the high-gain klystron design. The gain of the klystron FEL in this research was calculated with use of the coupled, self-consistent Lorentz-Maxwell equations. For high gain, the objective of the klystron configuration, the gain spectrum is found to be modified from the previously known

low-gain result. This is caused by the shifting of the optical phase during the gain process and is calculated for the first time. The effects derived are not obtainable from the Madey Theorem. The klystron saturation in strong nonlinear optical fields is also discussed. We make a comparison of the use of plasma theory and distribution functions, and the single particle approach. A manuscript of the research has been published, and the reference is below:

I. Boscolo and W. B. Colson, "Small Signal Gain Formula and Saturation in an Optical Klystron Free Electron Laser", Nuclear Instruments and Methods in Physics Research A237, 118 (1985).

#### **FEL Review Papers**

During the contracting period, two review articles were requested and written on FELs. The first was written for the annual FEL conference held in Castelgandolfo, Italy. It is a tutorial describing the theoretical work on FELs supported over a number of years by ONR. Extensions of the Lorentz-Maxwell theory are described that can be solved analytically, or numerically on a small computer. A brief discussion looks at high-gain collective effects, short pulse effects, harmonics, energy spread and emittance, transverse diffraction, and noise. The reference is

W. B. Colson, "Tutorial on Classical Free Electron Laser Theory", Nuclear Instruments and Methods in Physics Research A237, 1-9 (1985).

The second is a more general review of experiments and theory for the FEL written in cooperation with Andy Sessler of LBL. This paper is one of the most comprehensive papers now available on FELs. One table provides a description of all the FEL experiments, and another describes the electron accelerators that could be used to drive FELs. Specific experiments at LLNL, LANL, and Orsay are described in some detail to give the reader a more complete view of practical devices. The reference is

W. B. Colson and A. M. Sessler, "Free Electron Lasers", Annual Reviews of Nuclear and Particle Science 35, 25 (1985).

### Exotic Short-Pulse Propagation in the FEL

An FEL powered by an RF accelerator uses a series of short picosecond pulses injected into the FEL undulator in the oscillator configuration. We explored how the trapped-particle instability can alter the length of the short optical pulse and make it much shorter than the electron pulse. Typically, high-power saturation is reached after several hundred passes, and the FEL works in steady-state for an additional  $10^3$  to  $10^4$  passes. The current density of each short pulse  $j(z)$  is taken to be parabolic with the form  $j(z) = j(1 - 2z^2/\sigma_z^2)$  for  $|z| < \sigma_z/\sqrt{2}$  and  $j(z) = 0$  for  $|z| > \sigma_z/\sqrt{2}$ ; the FWHM  $\sigma_z$  is normalized to the slippage distance  $N\lambda$ . RF accelerators produce current densities that give values of the dimensionless current density  $j$  in the moderate range  $1 \rightarrow 100$  and  $\sigma_z = 1 \rightarrow 30$ . In addition to gain, there is loss on each pass due to mirror absorption and transmission; in the absence of gain, the optical power decays as  $e^{-n/Q}$  where  $n$  is the pass number. Usually,  $Q$  is from  $2 \rightarrow 200$ .

An important factor determining the optical pulse length is the matching of the electron pulse repetition frequency and the bounce frequency of the light pulse in the resonator  $2Sc$ . These frequencies must be closely synchronized so that each new electron pulse arrives at the beginning of the undulator simultaneous to the rebounding optical pulse. Define  $d$ , the "desynchronism," as the displacement between the pulses on each pass; if the mirrors are too close together by the distance  $\Delta S$ , then  $d = 2\Delta S/N\lambda$  where  $N$  is the number of undulator periods and  $\lambda$  is the optical wavelength. Maximum power is obtained at small  $d > 0$ . The desynchronism can be used to control the optical pulse length relative to the electron pulse length. When the desynchronism is small, the optical pulse is short; when the desynchronism is large, the optical pulse is long.

The general features of the trapped-particle instability in short-pulse FELs are briefly outlined below; many features have now been observed in experiments.

- At small  $d > 0$ , the FEL usually reaches power levels large enough to cause the trapped-particle instability. In this case, the optical pulse will be centered on the electron pulse, and will have sharp spikes due to the instability. This gives a broad, possibly chaotic, optical power spectrum, and a broad electron distribution. The trapped-particle instability adds frequency components that further shorten the already short optical pulse.
- At large  $d$ , the steady-state power is smaller due to the reduced coupling, and the trapped-particle instability is less likely to occur. The final optical power spectrum is narrow and in a single-mode; the final electron distribution is narrow due to the weak optical fields. Since the optical pulse is advanced by a large  $d$  on every pass, the center of the optical pulse may actually be ahead of the electron pulse. The desynchronism can be used to change the optical pulse length by as much as  $\times 10$  in an operating FEL.
- When  $d$  is in the intermediate range, we have often observed limit-cycle behavior in the simulations. In this case, the pulse continually changes shape while the trapped-particle instability creates new subpulses. A user-facility may be able to make use of this affect by providing users with both long and short pulses from a single machine. The changes take place on a time-scale like  $10\mu\text{s}$ .
- Increasing the current density  $j$  or the resonator  $Q$  increases the steady-state power; this increases the synchrotron frequency and the sideband gain. The addition of sideband power is cumulative, since the presence of a strong sideband again increases the steady-state power.

In Figure 1, a number of graphs show the results of a simulation where a steady-state optical pulse has evolved that is much shorter than the electron pulse. At the lower-left, the current density of a short pulse  $j(z + \tau)$  is shown at  $\tau = 0$  (black), and at  $\tau = 1$  (white) in the

calculational window of width  $W = 3$ . All longitudinal distances are normalized to the slippage distance  $N\lambda$  which can be in the picosecond range or smaller. The peak dimensionless current density is  $j = 50$ . The optical pulse amplitude  $|a(z, n)|$  is shown at the left evolving over  $n = 80$  passes through the resonator. The grey scale shows the peak field  $|a(z, n)| = 163$  in white, and zero field in black with two contours. On each pass, at  $\tau = 0$ , the optical wave is not driven because the new electron pulse from the accelerator is not bunched. At a later time  $\tau \leq 1$  when bunching develops, the electron pulse slips back, and drives the trailing edge of the light pulse. The light pulse is distorted on each pass because gain is preferentially deposited on the trailing edge of the pulse. Consequently, the center of the light pulse appears to be traveling slower than  $c$  even though in vacuum.

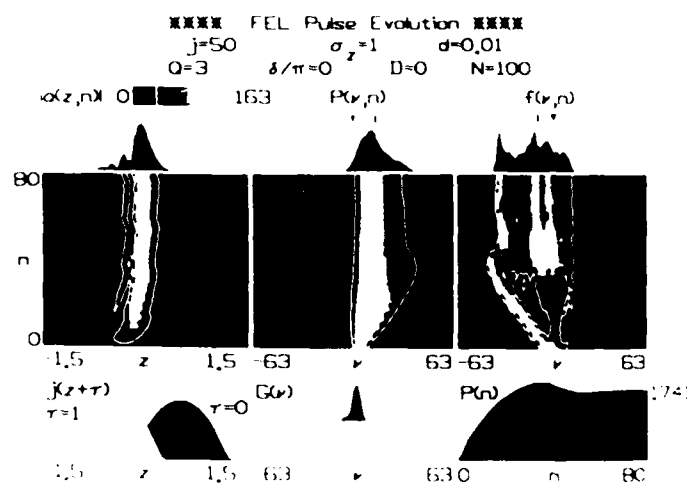


Figure 1. Simulation of a short, "spike" optical pulse; small  $d = 0.01$ .

The desynchronization in Figure 1. is  $d = 0.01$  and the advancing of the light pulse is seen in the first few passes. The gain and resonator loss at the mirrors, determined by  $Q = 3$  as defined above, combine to reshape the pulse until steady-state is achieved. The total power,  $P(n) = \int dz |a(z)|^2$  shown at the lower-right, has increased from the seed pulse to strong-field saturation. The short optical pulse shape gives the multimode power spectrum  $P(v, n)$  shown evolving in the middle. For reference, the single mode gain

spectrum  $G(\nu)$  is plotted at the bottom-center for  $j = 50$ . Mode competition keeps the fundamental optical spectrum near peak gain in weak fields, but strong field saturation will move peak gain to larger values of  $\nu$ . At saturation, the trapped electrons oscillate in the closed orbits of phase space on each pass. Over many passes, the frequency of the trapped particles mixes with the fundamental wavelength to produce sidebands. Note that the trapped-particle instability has, in this example, conspired to shorten the optical pulse and make the optical power spectrum  $P(\nu, n)$  actually broader than the FELs natural gain bandwidth. At the right is the evolution of the electron phase-velocity distribution  $f(\nu, n)$  taken at the end of the undulator  $\tau = 1$  on each pass; the final spread in phase velocity becomes broad as the field strength increases. The spread induced by the strong optical fields is roughly given by the peak-to-peak height of the separatrix  $4|a|^{1/2}$ .

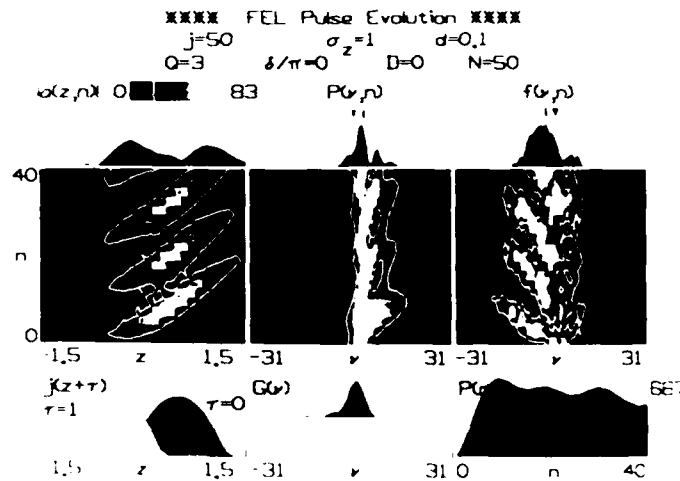


Figure 2. Simulation of a long, modulated optical pulse; large  $d = 0.1$ .

A second simulation is shown in Figure 2. with the same parameters except for the desynchronism of  $d = 0.1$ . The resulting pulse shape is dramatically different, and the simulation demonstrates many features that are found in the study. The optical pulse, in this case, is substantially longer than the electron pulse, and could be even longer with increased desynchronism. The saturated field strength is larger enough to cause the

trapped-particle instability and modulate the optical pulse envelope. The modulated pulse shaped continues to evolve forming a limit-cycle behavior. The net power, power spectrum, and electron spectrum all oscillate over several passes  $n$ . Note that power spectrum  $P(\nu, n)$  is now smaller than the natural gain spectrum  $G(\nu u)$ , and shows sideband structure due to the trapped-particle instability.

In conclusion, it was established that a wide range of optical pulse shapes can be found by changing the desynchronism  $d$  for a fixed dimensionless current density  $j$  and loss factor  $Q$ . For large  $j$  and  $Q$ , the optical and electron pulse shapes could differ more widely than with small  $j$  and  $Q$ . Experiments can easily reach the typical loss and gains required, and optical pulses can be easily made  $\times 10$  smaller and  $\times 10$  larger than the electron pulse length in the picosecond range. Greater divergence between the electron and optical pulses is possible but more difficult to control parametrically; a slight change make the resulting pulse and interaction chaotic and un-controllable. But, the controllable range is already exciting for future applications.

#### Optical Guiding in the FEL

A current topic in the FEL field during the contracting period was optical guiding. This effect describes the ability of the FEL interaction to focus light back into the electron beam. Historically, C. M. Tang and P. Sprangle (NRL) found that the low-gain FEL oscillator would modify the optical resonator mode so as to focus the light back into the electron beam. Later, G. Moore (U. of N.M.), and T. Scharlemann (LLNL) and A. Sessler (LBL) found that the effect can be much more dramatic in the high-gain regime; the light and electron beams could propagate over large interaction distances with good coupling. This is important for high-power, high-efficiency FEL amplifier designs. Natural diffraction normally provides a severe limitation to a long undulator length, but the "optical guiding" effect allows the electron beam and light to continue interacting over many Rayleigh lengths.

A description optical guiding was developed that does not rely on the fiber-optic analogy developed by Scharlemann and Sessler, nor the cubic dispersion relation used by Moore. The conceptual arguments do not make use of complicated simulations, but establish that the optical guiding effect comes from a large optical phase shift associated with the high  $j$  operating regime. In free space, the optical phase at the center of a wavefront evolves as  $\Delta\phi = -\Delta\tau/z_0$  for a small step  $\Delta\tau$ . The FEL interaction also modifies the wavefront as described in the dimensionless wave equation and pendulum equation. Consider a small electron beam in the middle of a co-propagating optical wave. If we average the wave equation over the transverse Gaussian mode area  $\pi z_0$  for a small step  $\Delta\tau$ , we can approximately recover the simple form with the new dimensionless current  $j \rightarrow jF$  where the "filling factor"  $F = \pi\sigma_\perp^2/\pi z_0$  is the ratio of the electron beam area to the optical mode area. The quantity  $jF \propto \rho F$  does not depend on the electron beam area, but only on the current within the optical mode. In the high-current regime where  $jF \gg 1$ , the optical phase evolves as  $\Delta\phi = (jF/2)^{1/3}\Delta\tau/2$ . We see that FEL interaction induces a phase shift that is opposite to that of natural diffraction, and therefore focuses the light back into beam along  $\tau$ .

Both the FEL change in amplitude and phase are such that they counter natural diffraction. To the extent that the FEL interaction on the optical field amplitude counters diffraction, this is termed "gain guiding". To the extent that the FEL interaction on the optical field phase counters diffraction, this is termed "phase guiding". Gain guiding is not surprising, but phase guiding is not necessarily common to all gain mediums.

In order for optical guiding to persist, the FEL interaction must continually compensate for the phase shift associated with free-space diffraction at each step  $\Delta\tau$ ; that is  $(jF/2)^{1/3}/2 \geq z_0^{-1}$ . The critical current density needed for optical guiding is then given by  $j^* \approx 16z_0^{-2}\sigma_\perp^{-2}$ . An FEL utilizing a small electron beam and a small optical wavefront (with a correspondingly short Rayleigh length), requires a larger current density for guiding. When the initial optical wavefront is focussed onto the electron beam, we would expect that

the filling factor  $F$  is not too small; we use  $\sigma_{\perp}^2 \approx z_0/2$  to write a simpler relation estimating the critical current density needed for optical guiding,

$$j^* \approx 32 z_0^{-3}$$

If the normalized Rayleigh length is small, say  $z_0 = \pi w_0^2 / L \lambda = 0.2$ , natural diffraction would spread the light over a large transverse area after the interaction length  $\Delta\tau = 1$ . Optical guiding can compensate in a typical high-current case where  $j \approx 10^4 > j^* \approx 4 \times 10^3$ . Note that the relations  $j^* \approx 16 z_0^{-2} \sigma_{\perp}^{-2}$  and  $j^* \approx 32 z_0^{-3}$  do not depend on the length of the undulator  $L$ , but express a comparison between the rates of natural diffraction and FEL focusing along  $\tau$ .

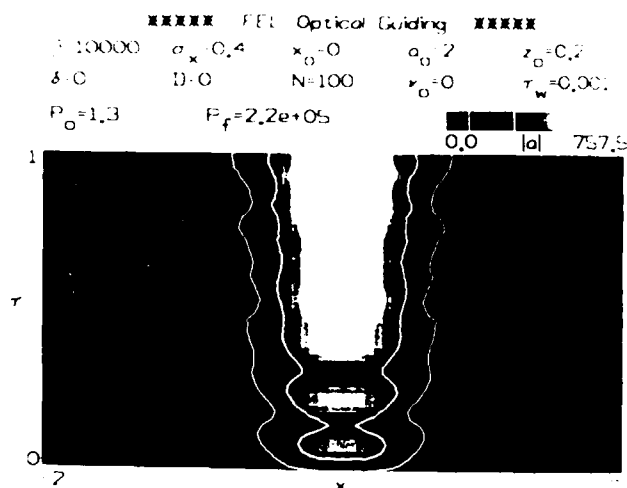


Figure 3. Optical guiding in the FEL.

Figure 3 shows a simulation that solves the full, diffracting wave equation, together with the pendulum equation, numerically to illustrate FEL optical focusing. The electron pulse is taken to be long, so that no  $z$  dependence is followed; in the transverse dimension, the electron beam is symmetric in  $x$ - $y$  with the parabolic shape  $j(r) = j(1 - r^2/2\sigma_{\perp}^2)$  for  $j > 0$ , and  $\sigma_x = 0.4$ . The peak density is  $j = 10000$ , and the initial phase velocity of the beam is  $v_0 = 0$  for maximum gain in the high-current case. A Gaussian optical mode is

focused near the beginning of the undulator at  $\tau_w = 0.001$  with a Rayleigh length  $z_0 = 0.2$ , and an initial field strength  $a_0 = 2$  at the center of the mode. The field amplitude  $|a(x, \tau)|$  grows along  $\tau$ , and reaches a peak value  $|a(0, 1)| \approx 750$  (white) a short distance along the undulator; points of zero field amplitude are shown as black. The scale at the top-right indicates the field amplitudes plotted in grey, and several contours following points of constant amplitude are superimposed. Without the FEL interaction, the mode would smoothly spread in  $z$  because of natural diffraction, but the contours show how the wavefront is focused back into the electron beam. This example is close to the ELF experiment at LLNL. In that experiment, a waveguide confined the optical mode so that optical guiding would not have been observed, but future visible experiments may be able to see the effect. There is also clear strong-field saturation in Figure 3 whereas the discussion above assumes weak optical fields to describe optical guiding. All that is needed for optical guiding is the optical phase shift that counters diffraction. Simulations show that the optical phase shift continues after saturation at the same rate as in weak fields. For this reason, experiments are expected to continue to use optical guiding to enhance efficiency in the saturated regime. The simulation in Figure 3 shows that optical guiding can continue after strong fields are reached.

#### Four-Dimensional, Self-Consistent FEL Theory

Historically, the pendulum equation approach to FEL theory was designed to clarify the electron dynamics and gain in the low-current regime. Later, the method was extended in order to solve the short-pulse problem in the Stanford SCA FEL. Multimode dependence in the longitudinal dimension was followed with field sites in the optical wave envelop and in the electron pulse. The extensions have continued, with ONR support over several years, so that a fully self-consistent, four-dimensional theory, following electron and optical quantities in  $(x, y, z, t)$ , could be developed. In this theoretical approach it would be possible, in principal, to include all relevant FEL effects. The development of spatial

periodic boundary conditions in the simulation of FEL longitudinal mode evolution is now being used extensively in the FEL community. Studies of the trapped-particle, sideband instability with long electron pulses must use this technique. The method has been employed at LANL in the FELIX code (B. McVey), at LLNL in the GINGER code (B. Fawley), and at Boeing/Spectra-Physics (D. Quimby). In the longitudinal dimension, the important physical process followed is the trapped-particle instability, while in the transverse dimensions, the concern is with diffraction, or optical guiding. The next few paragraphs outline some of the information regarding the multimode analysis used with periodic boundary conditions in order to document that part of the research effort.

The carrier wavelength provides the smallest relevant scale  $\lambda \approx \lambda_0 / 2 \gamma^2$  in the longitudinal dimension. The natural scale-length for multimode effects in the longitudinal dimension is determined by the natural gain spectrum width  $(1/2N)$ , or by electron-optical slippage distance; both estimates lead to the same important longitudinal distance  $N\lambda$ . A single point in the electron beam interacts with only  $N$  optical wavelengths during a pass through the undulator. Conversely, a single point in the optical wave envelope interacts with the electrons in a section of the beam  $N\lambda$  long.

An extension of the form of the optical field to multiple frequencies would make the optical field a function of the optical wavenumber  $k = \vec{k} \cdot \vec{z}$  in the longitudinal dimension. An alternative method is to follow multiple positions  $a(z)$  along the wave envelope. This is choice made in both GINGER and FELIX. The extension to spatial modes  $a \rightarrow a(z)$  is completely equivalent to an extension in longitudinal wavenumbers  $a \rightarrow a(k)$ . The concept of slippage in the FEL is somewhat more natural in the spatial modes representation. It is expected that the relevant mode spacing would be smaller than, but comparable to the gain bandwidth given by  $\Delta k/k \leq (2N)^{-1}$ . Normalize all longitudinal distances to the slippage distance for this discussion:  $z = Z/N\lambda$  where  $Z$  is the actual spatial coordinate, and  $z$  is the dimensionless longitudinal position. The complex optical field, the electron phase, and the electron dimensionless phase velocity must become a function of  $z$ :  $a \rightarrow a(z)$ ,  $v \rightarrow v(z)$ , and

$\zeta \rightarrow \zeta(z)$ . The number of sites needed in a particular problem is determined by the amount of detail to be followed in the optical spectrum. Recall that the FEL electron and wave equations assume a slowly varying optical amplitude and phase. They are, therefore, invalid equations of motion for describing a simulation that follows one optical wavelength adjacent to the next optical wavelength. The sampled sites in any given problem must be several to many optical wavelengths apart. This implies that the dimensionless  $z$  must have steps  $\Delta z \gg 1/N$ .

The electrons and light can evolve significantly in the slippage distance, or in one pass through the undulator. In fact, significant evolution of any quantity over this length scale  $N\lambda$  is the typical case. It is therefore necessary to sample several to many times in the distance  $N\lambda$  which implies that  $N^{-1} \ll \Delta z \ll 1$ . Typically, with  $N \approx 100$  this would imply that  $10^{-2} \ll \Delta z \ll 1$  which would be satisfied with by the choice  $\Delta z \approx 0.1$ . In a numerical simulation, the number of sites along the optical field envelope is finite, and the "window" containing those points is finite in length. The width of the window  $w$  is measured in units of the slippage distance  $N\lambda$  as are all other longitudinal dimensions; the window width  $w = 1$  corresponds to a length of one slippage distance in dimensionless units. When the number of sites in the window  $w$  is  $N_w$ , then the modes that are properly represented is given by the expression:

$$4\pi N \Delta \lambda_l / \lambda \approx \nu_l = \nu_0 - (2\pi / w) (l - N_w / 2) \quad \text{where } l = 0, 1, 2, \dots, N_w - 1$$

$w = N_w \Delta z$ , and  $\Delta \lambda_l$  is shift in wavelength away from the resonant wavelength  $\lambda$ . The mode spacing is given by  $\Delta \nu_l = 2\pi/w$ .

It appears that in most cases explored so far that  $w \rightarrow 1-10$  is adequate to characterize most free electron laser phenomena. The choice of  $w = 1$ , or 10, is determined by the kind of physics expected in the simulation. The window is typically only a few, to several, slippage distances long, since  $w$  is not a large number. This means that short pulse problems with lengths comparable to  $N\lambda$  are handled easily in such a window.

When the electron pulse and optical pulse are long compared to  $N\lambda$ , as in the case of an induction linac at LLNL, periodic boundary conditions can be imposed on all dynamical quantities at each end of the window  $w$ :  $\zeta(z - w/2) = \zeta(z + w/2)$ ,  $v(z - w/2) = v(z + w/2)$ , and  $a(z - w/2) = a(z + w/2)$ . The end-effects of the periodic boundary conditions are considered non-physical and inconsequential. The shorter window allows problems typical of the long pulse induction linacs at LLNL to be solved on existing computers. The electron pulse from the induction linac is from  $10^2$  to  $10^4$  slippage distances in length so that without periodic boundary conditions computation would not be practical.

The number of sample electrons is important in determining the amount of memory required in the computer. The longitudinal or transverse problems can each be handled on an IBM PC, but when combined, the code requires a Microvax II or CRAY level computer. The number of electrons at each site in the simulation can range from 20 to several thousand depending on the kind of problem being researched. As a general guide, FEL problems that saturate at power levels such that there is approximately one synchrotron oscillation, that is when the dimensionless optical field is  $|a| \approx 4\pi^2$  or less, then as few as 20 sample electrons might be adequate to represent the dynamics of the beam. If there is an initial energy or angular spread (emittance), then more are required. If the undulator design is tapered, then more are required because the electron phase acceleration spreads electrons over a wider range in phase space. In the high gain regime, the saturated power can be much greater than that required for one synchrotron oscillation so that more electrons may be necessary.

In the high current, high-gain regime ( $j \gg 1$ ), where the weak-field gain can be as large as  $10^{12}$ , the electrons and light may experience many e-foldings of growth in the slippage distance. Details of the interaction may not be "remembered" over the whole slippage distance, so that it is possible to use  $w < 1$  in a simulation. In another view, the gain spectrum for the high current case has a width  $\delta\nu \approx 4j^{1/6}$ , or  $\Delta k/k \approx 2j^{1/6}/\pi N$ , which can be significantly wider than the natural gain spectrum width  $1/2N$ . Several hundred time

steps with some sophisticated numerical integration scheme are usually necessary in the high current regime.

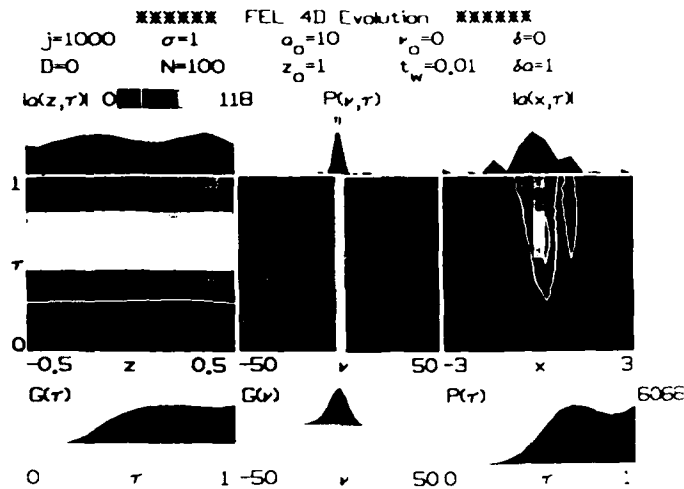


Figure 4. Fully four-dimensional FEL simulation results.

Figure 4. shows the results of a four-dimensional FEL simulation. In the longitudinal  $z$  dimension, periodic boundary conditions are used over one slippage distance with a window of length  $w_z = 1$  and 16 sites. In the transverse  $x$ - $y$  dimensions, an electron beam with a parabolic shape and size  $\sigma_x = \sigma_y = 1$  drives an optical wave. The peak current density is  $j = 10^4$  with the electrons in the beam starting at resonance  $v_0 = 0$ ; there are 16 electrons at each site where the current is non-zero. The initial optical wave is focussed near the beginning of the undulator at  $\tau_w = 0.01$  with a Rayleigh length of  $z_0 = 1$ ; the initial peak field strength is  $a_0 = 1$  and the transverse window has width  $w = 6$  with 16 sites in each dimension. Even with this minimal number of electrons and field sites in each dimension, the code runs for more than an hour on a Microvax II for a single pass through the undulator. The graphic output is a combination of figures shown in Figures 1, 2, and 3. At the bottom left is the evolution of gain  $G(\tau)$  and at the bottom right is the evolution of the net optical power  $P(\tau)$  along the undulator. At the middle, bottom is the single-mode gain spectrum  $G(v)$  for reference; above it is the evolution of the power spectrum  $P(v, \tau)$ . On the

left is the evolution of the longitudinal field magnitude  $|a(z, \tau)|$  in the window one slippage distance long; the final field structure is shown above the evolution with a grey scale for reference. On the right is the transverse optical field magnitude structure  $|a(x, \tau)|$  which remains focussed near the center of the window of width 6; the final transverse magnitude structure is shown at the top right. This kind of computer run can demonstrate the coupled effects in the longitudinal and transverse dimensions; for instance, the optical guiding of the transverse optical mode increases optical power and tends to create further sideband growth in the longitudinal optical field.

#### Coherence Development and Line Narrowing in the FEL

There has been relatively little research on the topic of line narrowing, or coherence development, in FEL theory. The FEL gain spectrum has a well-defined shape in the low-gain limit with a peak at  $v = 2.6$ . In the FEL oscillator, the optical field grows in power over many passes and develops coherence. In the first few passes, the optical power at each mode, identified by a particular phase velocity  $v$ , is provided by spontaneous emission. The spontaneous emission lineshape is the integral of the gain spectrum is symmetric in shape and has a width  $\Delta v \approx 2\pi$ . On each subsequent pass, the power in each mode at a  $v$  changes for three reasons: the spontaneous emission process adds power, the resonator mirrors and output coupling cause a loss, and the gain process with its antisymmetric shape increases or decreases power at a wavelength with phase velocity  $v$ . On one pass this can be described by

$$\Delta P(v) = S(v) + P(v)(G(v) - 1/Q)$$

where  $P(v)$  is the optical power in mode  $v$ ,  $S(v)$  is the spontaneous emission in mode  $v$  on each pass,  $\Delta P(v)$  is the change in the optical power,  $G(v)$  is the gain spectrum, and  $1/Q$  is the loss each pass taken to be independent of  $v$  here.

Line narrowing and coherence development in the FEL is the same as in an atomic laser except for the detailed shape of the gain and spontaneous spectra. In the first few passes after the oscillator is turned on, spontaneous emission results in a typical weak optical field of strength  $|a| \approx 10^{-4}$ . The field is initially incoherent with a coherence length of only  $N\lambda$ ; the spontaneous emission linewidth has is  $1/N$ . This coherence length is just barely long enough to support the classical gain process where electrons must bunch while passing through on slippage distance  $N\lambda$ . Over several hundred passes in the low gain regime, the coherence length can grow significantly longer than  $N\lambda$ , and the linewidth can become arbitrarily narrow.

In the limit of low gain, the optical power at each wavelength grows independently, the development of each mode can be expressed as a function of the second derivative of the gain spectrum expanded in a Taylor series about its maximum. Over many passes in the FEL oscillator, the wavelengths in an increasingly small region around the wavelength for maximum gain will fall behind in power leaving a narrow laser spectrum. A simple expression results that relates the FEL spectrum width  $\Delta\lambda/\lambda$ , the current density  $j$ , the number of undulator periods  $N$ , and the number of passes in the oscillator  $n$ . The spectral linewidth expected in an FEL oscillator after  $n$  passes is given by

$$\Delta\lambda/\lambda = 1/N(nj)^{1/2}$$

Eventually, at long evolution times, the spectrum is limited by practical or fundamental noise sources like vibrating optical components, or spontaneous emission.

Shown in Figure 5 is the line narrowing determined by iterating the above equation for the power spectrum change  $\Delta P(v)$  on each pass through the undulator in the FEL oscillator configuration. The spontaneous spectrum shape is shown at the bottom over a range of phase velocities  $-6 < v < 6$ . Above it is the gain spectrum shape with a peak at  $v = 2.6$ . Over many passes,  $n = 0 \rightarrow 60$ , the figure shows how the normalized optical spectrum  $P(v, n)/P_{\max}$  evolves from spontaneous emission into a narrower spectrum. The peak gain

is  $G = 0.135j$ , and the loss is determined by  $Q = 10$ . The final spectrum is centered around the phase velocity  $v = 2.6$  at peak gain, and has become much smaller than the spontaneous or gain spectra. The above formula for predicting the line narrowing after  $n$  passes would apply only after substantial narrowing has already occurred since it was derived by a Taylor expansion around a narrow spectrum. It is probably applicable for the last 10 to 20 passes.

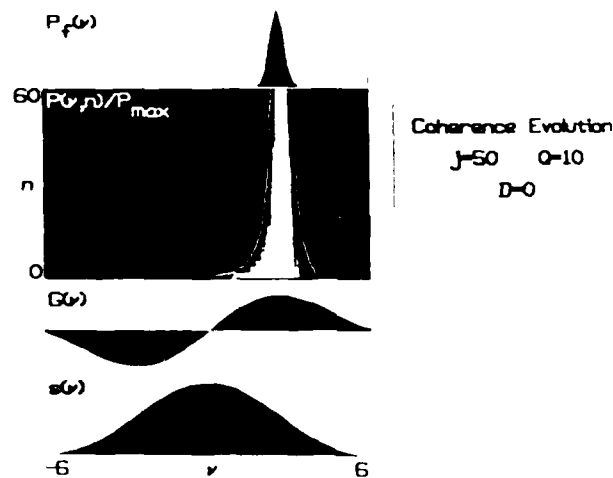


Figure 5. Line-narrowing in the FEL optical spectrum.

### The Trapped-Particle Instability $j$ - $Q$ Map for the FEL

The development of spatial periodic boundary conditions in the simulation of FEL longitudinal mode evolution is essential for solving long pulse FEL problems where the trapped-particle instability is expected. The technique evolved out of our work on short pulse propagation. A finite number of modes, and hence field points are determined by imposing periodic boundary conditions on the sites sampled. The simulations take much less memory and execution time than other methods, when the electron pulse length is long compared to the slippage distance.

Another advantage of the periodic boundary conditions is the parametric simplicity of the simulations describing FEL multimode evolution in the oscillator configuration. The physical input parameters are only the dimensionless current density  $j$  and the resonator loss described by  $Q$ . Other variables, like the number of sample electrons on each site, the number of sites, the initial optical field strength, or the initial phase velocity of electrons, should not affect the final steady-state result. In the oscillator configuration, the FEL initial conditions only provide a seed for starting the calculation and should not change the final steady-state optical spectrum, or electron distribution function. The initial conditions, number of sites, electrons, field strengths, etc. must be selected so that the final result represents the one that would be found in an experiment, and may be selected to find the result most efficiently, but otherwise, are not important. That leaves only  $j$  and  $Q$  to determine the multimode behavior of an FEL oscillator without short electron pulses. A single contour plot of the number of final modes as a function of  $j$  and  $Q$  is a universal description of all FELs.

It is the trapped-particle instability that creates the multimode behavior in the FEL oscillator configuration. When the trapped electrons oscillate through a synchrotron cycle, the FEL gain oscillates through one cycle. It is this oscillation in the driving phase, and the FEL gain that causes the trapped-particle frequency,  $\nu_s$ , to be imposed on the optical wave as it slips over electrons. The synchrotron or trapped-particle oscillation frequency is  $\nu_s = |\alpha|^{1/2}$  when written in dimensionless units. The sidebands appear at  $\nu_0 \pm \nu_s$ , so that the new FEL power is shifted from the fundamental wavelength by  $\Delta\lambda/\lambda = \nu_s/2\pi N$ . The shift has a simple interpretation;  $\Delta\lambda/\lambda =$  "the number of synchrotron oscillations"/ "the number of undulator periods."

Sidebands have been observed in high power RF FEL oscillators where the FEL mechanism has also influenced by short to moderately-short pulse effects as well. In the short-pulse FEL oscillator, the characteristics of the trapped-particle instability are affected by the synchronism, or desynchronism, between the rebounding optical pulse and the

successive electron pulses from the RF accelerator. The instability has only been observed when the FEL is near synchronism and the power in the resonator is largest. Increasing the current density  $j$  or the resonator  $Q$  increases the steady-state power, the synchrotron frequency, and the sideband gain. The addition of sideband power is cumulative, since the presence of a strong sideband again increases the steady-state power. When taper is introduced into the undulator design, the synchrotron frequency is only slightly modified, and the sideband gain is reduced. In simulations and experiments, the FEL oscillator runs for several hundred to thousands of passes through the interaction region. In that time, the stored optical wave "sees" many synchrotron oscillations, so that any sideband gain above threshold gives large growth from a small amount of noise. The resulting steady-state features are therefore not affected by the details of the noise source.

Only one experiment, the high power FEL at LANL, has now seen the trapped-particle sideband instability. It might have been observed earlier in the Stanford SCA FEL experiments, but was not; possibly, because the short-pulse effects dominated the interaction. From the experimental results, it is not at all clear that the synchrotron sideband instability is as prominent a problem as indicated by simulations. In the FEL amplifier, the input noise at the sideband frequency is important to the development of significant sideband power. This important factor cannot be found in any direct way by studying the FEL oscillator experiments, but the sideband gain can be assessed.

Two papers reviewed the properties of the trapped-particle instability in FEL oscillators and amplifiers. In these papers are the first examples of the trapped-particle instability in the FEL amplifier configuration. The references are

W. B. Colson, "The Trapped-Particle Instability in Free-Electron Laser Oscillators and Amplifiers", Nucl. Instr. & Methods in Phys. Res. A250, 168 (1986).

and

W.B. Colson, "The Effect of Electron Trapping in Free-Electron Laser Oscillators and Amplifiers", Proceedings of the 1985 International Conference on LASERs, Las Vegas CA (Dec. 1985).

Figure 6 shows the result of many simulations that make up the data in two  $j$ - $Q$  contour surfaces; each point on the surface is the result of a long multimode simulation over many passes of the oscillator. The range of current density explored on each contour surface is  $j = 2 \rightarrow 20$ , and the range of resonator loss is  $Q = 4 \rightarrow 20$ . The surface on the left is the total optical power  $P = \int |a|^2 dz$  in all modes after evolution to steady-state over many passes  $n = 20Q$  at each site. There are 16 sites in a longitudinal window one slippage distance long, or of unity length in dimensionless units. At each site there are 32 sample electrons, 512 electrons in all. The initial electron beam is monoenergetic at phase velocity  $v_0 = 4$ . The initial optical field amplitude is  $a_0 = 6$  with zero phase and a random modulation of value  $\delta a = 4$ . At each point in each surface, the only values physical values that matter are  $j$  and  $Q$ ; the other variables are judiciously selected to make the simulations valid and efficient.

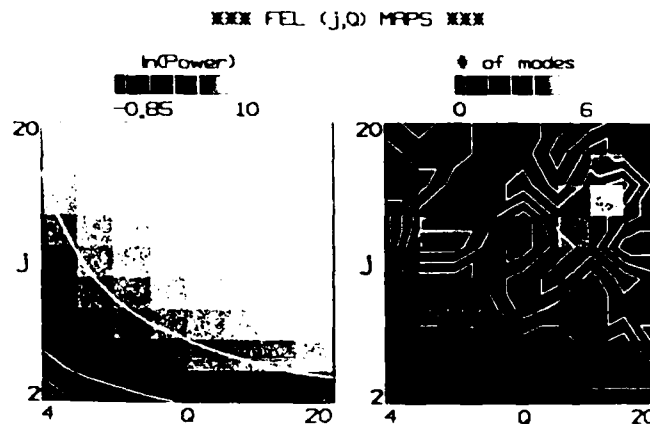


Figure 6. FEL  $j$ - $Q$  map of the trapped-particle instability.

The surface on the left of Figure 6 plots  $\ln(P)$  as a function of  $j$  and  $Q$ . Increasing either  $j$  or  $Q$  increases the optical power smoothly  $P$  in this range. A grey scale is given at the top of the surface with contours for quantitative evaluation. At low values of  $j$  and  $Q$ , the FEL is below threshold and the power decays to a small value. When  $j \approx Q \approx 20$ , the power increases to  $P \approx 2.2 \times 10^4$ ; the corresponding field amplitude at saturation for this  $j-Q$  value is then  $|a| = P^{1/2} \approx 148$ . The synchrotron frequency is  $\omega_s = |a|^{1/2} \approx 4\pi$  giving two synchrotron oscillations of trapped-electrons in a single-pass through the FEL undulator. This intense field amplitude will result in sideband mixing and chaos field structure as shown in the second contour map on the right.

The right-hand surface shows the number of optical modes resulting from each simulation. The number of modes ranges from 1 to 6, and generally increases when either  $j$  or  $Q$  is increased. The number of modes does not steadily increase with  $j-Q$ , however; there may be some features that require further study, but we can see from individual simulations that the optical field becomes chaotic after just a few sideband modes appear. This may, in part, explain the chaotic features in the modal  $j-Q$  surface. On the other-hand, if there are actually special values of  $j-Q$  that avoid the trapped-particle instability, or pass through an evolutionary state where there is single mode behavior, this would have important high-power FEL applications.

#### **Invention (Patent) Report:**

None

END

DATE

FILMED

5-88  
DTIC